ECCM '99
European Conference on
Computational Mechanics
August 31 – September 3
München, Germany

Application of continuum laws in discontinuity analysis based on a regularised displacement discontinuity

G. N. Wells
Faculty of Aerospace Engineering / Koiter Institute Delft
Delft University of Technology, The Netherlands
e–mail: g.wells@ct.tudelft.nl

L. J. Sluys
Faculty of Civil Engineering and Geosciences / Koiter Institute Delft
Delft University of Technology, The Netherlands
e–mail: l.j.sluys@ct.tudelft.nl

Key words: Strong discontinuity, embedded crack, plasticity, damage.

Abstract. *The application of continuum constitutive laws in embedded strong discontinuity analysis is examined. By adopting a regularised discontinuity (approximating the unbounded strain field resulting from a displacement jump with a bounded function), the strain field in a body is always bounded, hence continuum laws can be applied. However, this must be done with some caution since the 'fictitious' strain state at the discontinuity can lead to spurious behaviour that does not arise in the conventional application of classical constitutive laws. Particularly addressed is stress locking as a function of the displacement regularisation in some plasticity models. It is also shown that the regularisation function can have a serious impact on convergence behaviour for some types of constitutive models.*

1 Introduction

The inclusion of discontinuities into the classical continuum has attracted significant attention recently as a means to overcome deficiencies of the classical continuum when applied to softening solids, while still applying conventional continuum constitutive laws. The mesh sensitivity of conventional continuum models for failure analysis is well recognised. At the onset of strain softening, the classical rate-independent continuum equations become ill-posed [1]. With mesh refinement, strains localise in collapsing bands, resulting in the limiting case of failure with zero energy dissipation [2]. To remedy this, *mesh* regularisation techniques, often based on fracture energy, have been applied. However, these techniques introduce physically meaningless measures of the spatial discretisation (sometimes known as the 'crack bandwidth') to the constitutive equations, rather addressing the underlying deficiency in the continuum description.

Enhanced continuum (gradient and non-local) models have proved successful in overcoming mesh dependency in softening materials [3–6]. The inclusion of a material internal length scale to the continuum description means that localised bands do not collapse upon mesh refinement. However, a common feature of enhanced continuum models is the need for a very fine mesh in the failure zone (usually several elements across) in order to capture the high strain gradients. This requires prior knowledge of where localisation bands will form for practical problems, limiting application in real-scale problems, especially in three dimensions.

The embedment of discontinuities within finite elements offers a hybrid approach between smeared continuum and discrete failure models. By inserting a discontinuity within an element, a discrete type phenomena can be modelled in a continuum framework. Unlike discrete approaches, the direction of the discontinuity is determined solely by the stress or strain field, avoiding mesh alignment dependency and the need for special mesh realignment techniques. Unlike smeared, classical continuum models, no mesh dependent parameters are used in the constitutive relations in order to preserve the energy dissipation characteristics of the material. In the case of models where extra shape functions are added to model a discontinuity, the kinematic ability of elements to reproduce the real deformation modes is superior to smeared approaches, avoiding some of the kinematic difficulties and spurious behaviour associated with smeared crack models.

The application of continuum based laws for *weak* discontinuities (discontinuity in the strain field) follows naturally from the bounded strain field. The introduction of a *strong* discontinuity (discontinuity in the displacement field) immediately leads to an unbounded strain field at the discontinuity, suggesting the need for a discrete (traction-displacement) law. It has been shown however, by examining continuum models for softening materials that continuum constitutive models are compatible with unbounded strains under certain conditions [7, 8]. Here the practical implications and some difficulties of applying continuum laws for discontinuity analysis are examined, along with some solutions. Attention is focused on two different constitutive models for mode-I type failure; an isotropic damage model and a multi-surface Rankine plasticity model. It is shown that issues arise specific

to each model, often owing the strain (damage) and the stress (plasticity) driven nature of each model.

2 Kinematics of the discontinuity

First consider a body crossed by a physical discontinuity (Figure 1). The displacement field of a body containing a discontinuity can be decomposed into two parts; a continuous ($\hat{\mathbf{u}}(\mathbf{x},t)$) and a discontinuous ($\mathcal{H}_{\Gamma_d}[\mathbf{u}](\mathbf{x},t)$) component. The jump in displacement is provided via the Heaviside function ($\mathcal{H}_{\Gamma_d}$), centred on the discontinuity, operating on a continuous function $[\mathbf{u}](\mathbf{x},t)$. The magnitude of the displacement jump is given by the magnitude of $[\mathbf{u}](\mathbf{x},t)$ at the discontinuity.

$$\mathbf{u}(\mathbf{x},t) = \hat{\mathbf{u}}(\mathbf{x},t) + \mathcal{H}_{\Gamma_d}[\mathbf{u}](\mathbf{x},t) \tag{1}$$

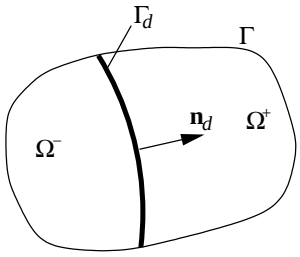

Figure 1: Body containing a discontinuity

The corresponding strain field can then be found by calculating the gradient of (1).

$$\boldsymbol{\varepsilon}(\mathbf{x},t) = \boldsymbol{\nabla}^s\hat{\mathbf{u}} + \mathcal{H}_{\Gamma_d}(\nabla^s[\mathbf{u}]) + \delta_{\Gamma_d}([\mathbf{u}]\otimes\mathbf{n}_d) \tag{2}$$

where $\mathbf{n}_d$ is the normal to the discontinuity and δ_{Γ_d} is the Dirac-delta distribution centred on Γ_d.

Differentiation of the Heaviside function leads to the appearance of the unbounded Dirac-delta distribution in the strain field expression. The strain field can be grouped into bounded (regular) and unbounded parts [7, 8].

$$\boldsymbol{\varepsilon}(\mathbf{x},t) = \underbrace{\bar{\boldsymbol{\varepsilon}}}_{\text{bounded}} + \underbrace{\delta_{\Gamma_d}([\mathbf{u}]\otimes\mathbf{n}_d)}_{\text{unbounded}} \tag{3}$$

3 Continuum constitutive laws

The application of continuum constitutive laws relies primarily on the physical justification that unbounded strain fields are notionally possible and that unbounded stresses are impossible. That is, irrespective of the strain field, the stress field is bounded at all times.

From a physical point, an unbounded strain field arises naturally in the case of a displacement discontinuity. As a result of the natural stress boundedness requirement, the

application of continuum constitutive laws is conditional upon the chosen constitutive law exhibiting a softening branch. Any hardening behaviour at the discontinuity would lead to an unbounded stress field.

The general formulation of isotropic, strain softening damage and plasticity models for application in discontinuity analysis is shown here.

3.1 Plasticity

For plasticity models, it is simplest to begin from the inverse of the classical elasto-plastic tangential stiffness matrix for isotropic hardening/softening associative plasticity (hardening modulus (H) is not equal to zero)

$$\dot{\boldsymbol{\varepsilon}} = \left((\mathbf{D}^e)^{-1} + \frac{1}{H} \mathbf{m}\mathbf{m}^T \right) \dot{\boldsymbol{\sigma}} \tag{4}$$

with

$$\mathbf{m} = \frac{\partial f}{\partial \boldsymbol{\sigma}} \tag{5}$$

where $\mathbf{D}^e$ is the elastic tangent matrix and f the yield function. The expression for the strain field in (3) can be differentiated with respect to time, then substituted into equation (4).

$$\underbrace{\dot{\bar{\boldsymbol{\varepsilon}}}}_{\text{bounded}} + \underbrace{\delta_{\Gamma_d} \mathbf{n}_d [\dot{\mathbf{u}}]}_{\text{unbounded}} = \underbrace{(\mathbf{D}^{-1})^T \dot{\boldsymbol{\sigma}}}_{\text{bounded}} + \frac{1}{H} \underbrace{\mathbf{m}\mathbf{m}^T \dot{\boldsymbol{\sigma}}}_{\text{bounded}} \tag{6}$$

For the equality in equation (6) to be true, the unbounded term in (6) containing the Dirac-delta distribution must be cancelled by the hardening modulus. This can be done simply by distinguishing between the *hardening modulus* (H) and the *intrinsic hardening modulus* ($\bar{H}$) [7, 8] and relating the two by

$$\frac{1}{H} = \delta_{\Gamma_d} \frac{1}{\bar{H}} \tag{7}$$

The intrinsic softening parameter can be found easily by integrating the one dimensional stress-displacement relationship (shown for linear softening in Figure 2), giving

$$\bar{H} = -\frac{f_t^2}{2G_f} \tag{8}$$

Note the similarity between equation (7) and the softening modulus used in smeared crack bandwidth formulations, where the measure of element size has been replaced by the inverse of the Dirac-delta distribution. Effectively, if the inverse of the softening modulus has a distributed form of the Dirac-delta distribution, the stress field will always be bounded (at least for the one-dimensional case shown in Figure 2).

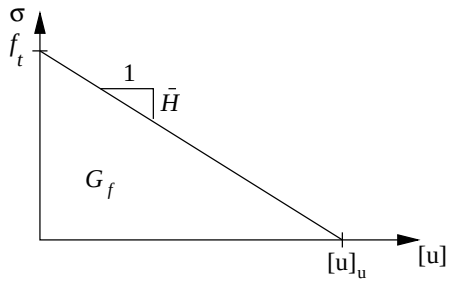

Figure 2: 1-D linear stress-displacement relationship

3.2 Continuum damage

Considering an elasticity based isotropic damage model where all damage is represented by a single scalar variable (ω), the stresses at a point($\boldsymbol{\sigma}$) can be described in terms of the damage parameter, the elastic tangent matrix and the strains at that point.

$$\boldsymbol{\sigma} = (1-\omega)\mathbf{D}^e\boldsymbol{\varepsilon} \tag{9}$$

For the analysis of concrete, a principal strains based equivalent strain measure, proposed by [9] is used for the internal history-dependent parameter (κ)

$$\kappa = \max\left(\kappa_0, \tilde{\varepsilon}\right) \tag{10}$$

$$\kappa_0 = \frac{f_t}{E} \tag{11}$$

$$\tilde{\varepsilon} = \sqrt{\sum_{i=1}^{3} < \varepsilon_i >^2} \tag{12}$$

where ε_i are the principal strains and $< \cdot >$ is equal to $(\cdot)$ if $\varepsilon_i > 0$ and zero if $\varepsilon_i \leq 0$.

For a linear softening law (Figure 3), the damage variable can be expressed in terms of the internal variable as

$$\omega(\kappa) = \begin{cases} \left(\frac{1}{1+H}\right)\left(1-\frac{\kappa_0}{\kappa}\right) & \kappa < -\frac{1}{H}\kappa_0 \\ 1 & \kappa \geq -\frac{1}{H}\kappa_0 \end{cases} \tag{13}$$

where the softening parameter $H = -\kappa_0/\kappa_u$.

It is convenient now to express the equivalent strain expression in (12) in terms of stresses [7]. This can be done simply since the stresses and strains are related by the isotropic elastic tangent matrix

$$\tilde{\varepsilon} = \left(\frac{1}{1-\omega}\right)\tilde{\varepsilon}_\sigma = \frac{1}{1-\omega}\sqrt{\sum_{i=1}^{3} < \frac{1}{E}(\sigma_i - \nu\sigma_j - \nu\sigma_k) >^2} \tag{14}$$

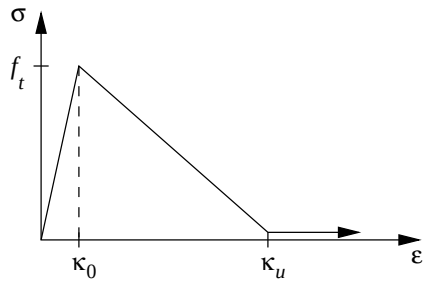

Figure 3: Linear softening diagram

where $\sigma_{i,j,k}$ are the principle stresses. Substitution of equation (14) into the damage parameter expression (13) then yields

$$\frac{\omega}{1-\omega} = \frac{1}{H}\left(1 - \frac{\kappa_0}{\kappa_\sigma}\right) \tag{15}$$

where $\kappa_\sigma = \max(\kappa_0, \tilde{\varepsilon}_\sigma)$. Equation (9) can then be rearranged such that

$$\left(1 - \frac{\omega}{1-\omega}\right)\boldsymbol{\sigma} = \mathbf{D}^e\boldsymbol{\varepsilon} \tag{16}$$

Substituting the strain field from equation (3) into (16) leads to

$$\underbrace{\boldsymbol{\sigma}}_{\text{bounded}} + \left(\frac{\omega}{1-\omega}\right)\boldsymbol{\sigma} = \underbrace{\mathbf{D}^e\bar{\boldsymbol{\varepsilon}}}_{\text{bounded}} + \underbrace{\delta_{\Gamma_d}\mathbf{D}^e\mathbf{n}_d[\mathbf{u}]}_{\text{unbounded}} \tag{17}$$

which can be further rearranged collecting the terms relating to the continuous part of the body on one side and the discontinuous part of the body on the other side.

$$\boldsymbol{\sigma} - \mathbf{D}^e\bar{\boldsymbol{\varepsilon}} = \delta_{\Gamma_d}\mathbf{D}^e\mathbf{n}_d[\mathbf{u}] - \left(\frac{\omega}{1-\omega}\right)\boldsymbol{\sigma} \tag{18}$$

Since the LHS of equation (18) is bounded, the unbounded term on the RHS containing the Dirac-delta distribution must be cancelled by the term containing the damage parameter. Substituting the expression for the damage parameter in equation (15) into equation (18), the strain field can be made bounded by giving the softening parameter the form [7]

$$\frac{1}{H} = \delta_{\Gamma_d}\frac{1}{\bar{H}} \tag{19}$$

where $\bar{H}$ is the intrinsic softening parameter. For damage models, $\bar{H}$ can be found by integrating the energy dissipation rate for a 1-D softening bar.

$$G_f = \int_{\kappa_0}^{\kappa_u} \frac{1}{2}E\kappa^2\frac{\partial\omega}{\partial\kappa}\,d\kappa \tag{20}$$

For linear softening this gives an intrinsic softening parameter

$$\bar{H} = -\frac{f_t^2}{2G_f E} \tag{21}$$

Again, the softening parameter resembles the softening parameter for smeared type continuum models.

4 Effect of displacement jump regularisation

In the previous section it was shown that by specially constructing the softening parameter, continuum constitutive laws can be applied. Now, for numerical simulation, Dirac-delta distribution and the resulting unbounded strains at the discontinuity must be approximated. To do this, the Dirac-delta distribution is approximated by a function that approaches the Dirac-delta distribution, thereby regularising the displacement jump and bounding strains at all locations [7, 10].

$$\delta \approx \frac{1}{k} \tag{22}$$

The approximation of the Dirac-delta distribution (22) allows the numerical application of continuum constitutive laws, where k can be considered as the width of an *inner softening band*. From the form of the hardening modulus for plasticity (7) and damage (19), constitutive laws formulated for fracture energy regularised smeared models can be applied without modification, with the 'crack bandwidth' simply replaced by k. The strain field in the softening band is given in terms of displacements at the discontinuity as

$$\boldsymbol{\varepsilon}_d = \frac{1}{k}(\mathbf{n}_d[\mathbf{u}]) \tag{23}$$

The effect of the approximation across the discontinuity deserves some investigation. In the following sections the effect of the displacement jump regularisation is investigated for a Rankine plasticity model and the isotropic damage model, outlined in Section 3.2, for mode-I type problems.

4.1 Stress locking

For modelling materials where mode-I type failure is dominate (such as concrete), Rankine plasticity has been applied in smeared crack modelling [11, 12] and has been shown to largely overcome the spurious stress locking inherent in fixed crack models [13]. The multi-surface plasticity based model performs well in tension dominated problems where the principle stress axes rotate since the yield surface is constructed in the principle stress space, effectively allowing rotation of the yield surface in the global coordinate system. Upon the introduction of a discontinuity, an element is immediately given some directional bias which can result in stress locking. This effect was examined by [14] for a Rankine

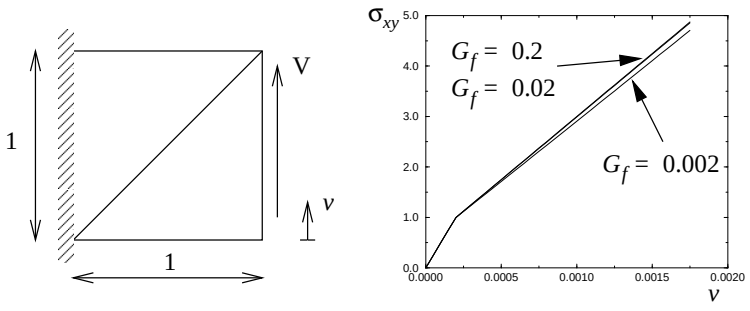

Figure 4: Shear panel and shear-displacement response for varying G_f

model, with attention focused on stress locking as a consequence of an element being unable to kinematically produce the real deformations (*kinematic* stress locking). The source of this problem and solution strategies are similar to those for smeared fixed crack models [13].

The problem of kinematic stress locking in embedded models with fixed discontinuities is not unique to models using continuum constitutive laws. However, the application of a regularised discontinuity in combination with Rankine plasticity introduces a second source of stress locking that is dependent on the regularisation function (22), arising from the fictional nature of the strain field at the discontinuity (k-type stress locking). The strain field at the discontinuity is proportional to the displacements at the discontinuity (the objective measure of deformation) and inversely proportional to the width of the discontinuity band k. So, as k decreases (approaching the Dirac-delta distribution), the strains increase. This effect is then accounted for by the adjustment of the softening modulus. However, if the chosen constitutive law does not allow softening in *all* directions, very small displacements at the discontinuity result in very large strains at the discontinuity, leading to spurious stress development. This is in contradiction to the condition at the beginning of Section 3 that the constitutive law must exhibit a softening branch.

For Rankine plasticity, the response of a square patch in pure shear is examined (Figure 4) with the following material parameters: $f_t = 1.0\,\text{MPa}$, $E = 10 \times 10^3\,\text{MPa}$, $\nu = 0.2$ and linear softening. Since the Rankine yield surface is in the principle stress space, there is no bound on the shear stresses that can develop. The shear stress–displacement response in Figure 4 shows that no shear softening occurs, hence the shear stresses that can develop are unbounded, with the response insensitive to the fracture energy parameter. In smeared analysis of tension dominated problems, the shear strains are usually small, hence large shear stresses do not develop and stress locking is significant.

As a result of the inability of the Rankine model to soften in shear, for decreasing k, very small sliding motions at the discontinuity result in very large shear stresses (unlike the isotropic damage model in Section 3.2 which does not exhibit the k-dependent stress locking since the damage parameter operates on both the tensile stiffness and the shear modulus, allowing softening in shear). In realistic type problems, the spurious shear

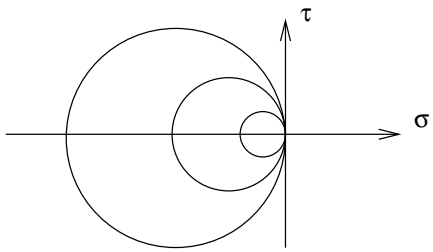

Figure 5: Stress states in the discontinuity when fully softened

stresses that develop at the discontinuity can be of the same order of magnitude as the inverse of k. This build up of very large spurious stresses can then lead to unpredictable results and a loss of robustness. A simple Mohr circle in Figure 5 shows how the fictional strain state at the discontinuity can lead to the development of both large shear and compressive stresses in the fully softened state for tension problems.

It has been shown that for simple one dimensional bars, the load displacement response is independent of the value of k, conditional of course on k being smaller than the element [15]. The k-type stress locking arises only in more complex examples, raising the question of why a small value for k is required. In order to use a large value of k (which usually results in improved convergence behaviour), it is necessary to show that the result is independent of the regularisation function (22). Without examining a particular problem for various values of k, it is not possible to test for the influence of the regularisation and any spurious effects.

There are two possible solutions for k-type stress locking with a regularised discontinuity. The first, an improved constitutive model that allows both separation and sliding type deformations. The addition of a lower bound to the Rankine yield surfaces would limit the shear stress that could develop, although since it is still formed in the principle stress space does not directly address the mode-II deficiency. The second solution is to allow extra kinematic enhancement by allowing multiple or rotating discontinuities.

Unlike for kinematic type stress locking, allowing multiple cracks is not a feasible solution for k-type stress locking. With decreasing k and Rankine plasticity, severe stress locking can occur with only very minor rotation of the principle axes. For a multiple crack model, as k decreases the threshold angle for the introduction of new discontinuities to avoid stress locking approaches zero. For this reason, allowing rotation of the discontinuity is examined. To compare fixed and rotating discontinuities using Rankine plasticity, a non-symmetric notched specimen, previously examined by [16], is analysed with varying k (Figure 6). The material parameters adopted are: $f_t = 1.0\,\mathrm{MPa}$, $E = 10 \times 10^3\,\mathrm{MPa}$, $\nu = 0.2$ and $G_f = 0.02\,\mathrm{Nmm/mm^2}$ (exponential softening). Figure 7a shows the increasing stress locking effect with decreasing k for the fixed discontinuity model. By allowing rotation of the discontinuity, in this case k-type stress locking is avoided. Figure 8 shows that the discontinuity directions in most elements for the fixed and rotating models are indistinguishable, but allowing rotation has a significant effect on the load-displacement behaviour. Since the rotations of the discontinuity are so small, a multiple crack model

could not alleviate the k-dependent stress locking.

It can be seen that allowing small rotations of the discontinuity alleviates a deficiency of the Rankine plasticity model when coupled with a regularised discontinuity. However, it is not a reasonable solution to kinematic type stress locking for the finite element model used here (based on that of [7]) since large rotations of the discontinuity are necessary, making the model unstable as the discontinuity passes from one side of an element node to the other [15, 17]. To fully alleviate stress locking when applying Rankine plasticity in a rotating stress field, a combined multiple-rotating crack approach is required.

4.2 Tangent operator and stability

For plasticity, the classical elasto-plastic tangent operator can be obtained by inverting equation (4) using the Sherman-Morrison formula.

$$\dot{\boldsymbol{\sigma}} = \underbrace{\left(\mathbf{D}^e - \frac{\mathbf{D}^e\mathbf{m}\mathbf{m}^T\mathbf{D}^e}{H + \mathbf{m}^T\mathbf{D}^e\mathbf{m}}\right)}_{\mathbf{D}^{ep}} \dot{\boldsymbol{\varepsilon}} \tag{24}$$

Notice that $\mathbf{D}^{ep}$ does not contain any terms differentiated with respect to the strain field. For efficient numerical calculations, a consistently linearised tangent operator must be used in forming the element stiffness matrix. The tangent consistent with the backward Euler integration scheme (for the Rankine model applied, see [12]) can be formed with only the plastic multiplier (λ) dependent directly on the strain field. As a result, robustness of the numerical scheme is not compromised at the introduction of a discontinuity with decreasing k.

Similarly, a tangent relating stress rate and strain rate for the isotropic damage formulation can also be derived. Differentiating equation (9) with respect to time, it can be shown

$$\dot{\boldsymbol{\sigma}} = \underbrace{\mathbf{D}^e\left((1-\omega)\mathbf{I} - \frac{\partial\omega}{\partial\kappa}\boldsymbol{\varepsilon}\frac{\partial\tilde{\varepsilon}}{\partial\boldsymbol{\varepsilon}}\right)}_{\mathbf{D}^c}\dot{\boldsymbol{\varepsilon}} \tag{25}$$

It is interesting now to examine the form of the tangent matrix in (25). Recalling the approximation of the Dirac-delta distribution, as k approaches zero, at the onset of inelastic

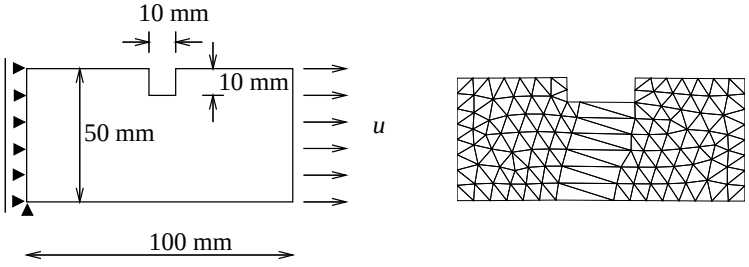

Figure 6: Notched specimen and deformed mesh

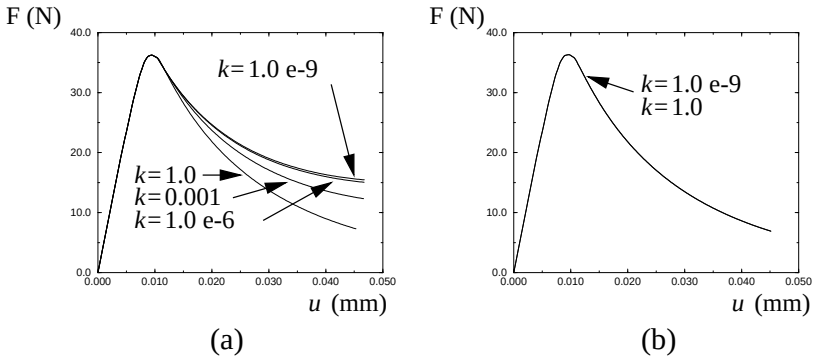

Figure 7: Sensitivity to k for fixed (a) and rotating (b) discontinuities

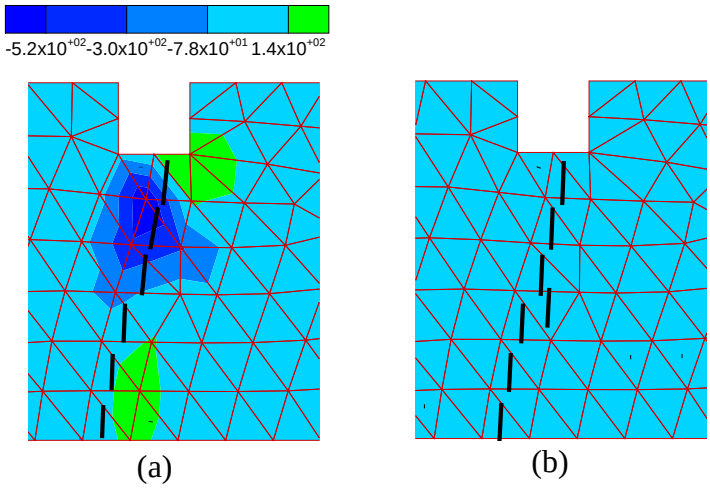

Figure 8: Embedded cracks and shear stresses for fixed (a) and rotating (b) models for $k = 1.0 \times 10^{-7}$

deformation, the damage parameter ω jumps from zero to a value approaching unity to maintain a bounded stress field. As a result, the derivative of the damage parameter with respect to the internal variable $(\partial\omega/\partial\kappa)$ starts from the 'continuum' value at the introduction of a discontinuity and after the first iteration then approaches zero. The consequence is that with decreasing k, it becomes increasingly difficult to find a converged solution at the end of the first time step after the introduction of a discontinuity. This can be examined more closely by expanding the expression within the brackets for the consistent tangent (plane stress case).

$$\mathbf{D}^c = \mathbf{D}^e \left(\begin{bmatrix} (1-\omega) & 0 & 0 \\ 0 & (1-\omega) & 0 \\ 0 & 0 & (1-\omega) \end{bmatrix} - \frac{\partial \omega}{\partial \kappa} \begin{bmatrix} \varepsilon_x \frac{\partial \tilde{\varepsilon}}{\partial \varepsilon_x} & \varepsilon_x \frac{\partial \tilde{\varepsilon}}{\partial \varepsilon_y} & \varepsilon_x \frac{\partial \tilde{\varepsilon}}{\partial \gamma_{xy}} \\ \varepsilon_y \frac{\partial \tilde{\varepsilon}}{\partial \varepsilon_x} & \varepsilon_y \frac{\partial \tilde{\varepsilon}}{\partial \varepsilon_y} & \varepsilon_y \frac{\partial \tilde{\varepsilon}}{\partial \gamma_{xy}} \\ \gamma_{xy} \frac{\partial \tilde{\varepsilon}}{\partial \varepsilon_x} & \gamma_{xy} \frac{\partial \tilde{\varepsilon}}{\partial \varepsilon_y} & \gamma_{xy} \frac{\partial \tilde{\varepsilon}}{\partial \gamma_{xy}} \end{bmatrix} \right) \tag{26}$$

For the simple case of a bar loaded in tension in the x-direction, the internal variable (κ)

and the strain in the x-direction are equal and $\partial\tilde{\varepsilon}/\partial\varepsilon_x$ is equal to unity. Substituting the expression for the damage variable (equation (13)) and its derivative with respect to the internal variable, the (1,1) component of the expression inside the brackets of (26) can be expressed in terms of the internal variable.

$$(1-\omega) - \frac{\partial\omega}{\partial\kappa}\,\kappa \;=\; 1 - \frac{1}{1+H} + \frac{1}{1+H}\left(\frac{\kappa_0}{\kappa}\right) - \frac{1}{1+H}\left(\frac{\kappa_0}{\kappa^2}\kappa\right) \;=\; 1 - \frac{1}{1+H} \tag{27}$$

Effectively, the sudden jump in ω is cancelled by the sudden jump in the derivative of the ω with respect to the internal variable. For this simple case, the (1,1) component is constant.

Next the (2,1) component is examined.

$$-\frac{\partial\omega}{\partial\kappa}\,\varepsilon_y \;=\; -\frac{1}{1+H}\left(\frac{\kappa_0}{\kappa^2}\right)\,\varepsilon_y \tag{28}$$

Considering the discontinuous component of the strain field across the discontinuity, (equation (23)), for this case of a bar loaded in the x-direction,

$$\kappa = \varepsilon_x = \frac{1}{k}[u_x] + \varepsilon_x^{\text{regular}} \tag{29}$$

it can been seen that the the (2,1) term is proportional to k^2.

From equation (28), the $\partial\omega/\partial\kappa$ term is not complemented by the damage parameter. At the introduction of a discontinuity, $[\mathbf{u}]$ is zero, so $\partial\omega/\partial\kappa$ is independent of k. At the next iteration after the introduction of a discontinuity ($[\mathbf{u}]$ is non-zero), there is a jump in (28), proportional to the square of k. As a result, at the first iteration *after* a discontinuity is introduced, there is a sudden jump in the strain field resulting in a sudden jump in components of the consistent tangent.

The sudden jump in strains and resulting jump in some components of the consistent tangent has a detrimental effect on the convergence behaviour in the first increment when a discontinuity is introduced, as k decreases. It can also lead to oscillations of the Newton-Raphson scheme within the first increment when the discontinuity is introduced. If a discontinuity is introduced to an element at the first iteration, then upon the second iteration a redistribution of forces results in no inelastic deformation, the sudden changes in the tangent matrix can result in oscillating convergence behaviour.

The result is that as k decreases, the step size of the Newton-Raphson scheme must also decrease[1] in order to capture intermediate values of ω between zero and very close to unity (then also intermediate values of $\partial\omega/\partial\kappa$ between the initial value and close to zero are captured). It is possible to examine the effect of reducing k by analysing a unit patch with a constant displacement increment and varying k. The patch of three-noded

[1] In some cases, decreasing step sizes leads to a deterioration of convergence behaviour. The application of large increments can allow the numerical scheme to 'step' over the oscillations.

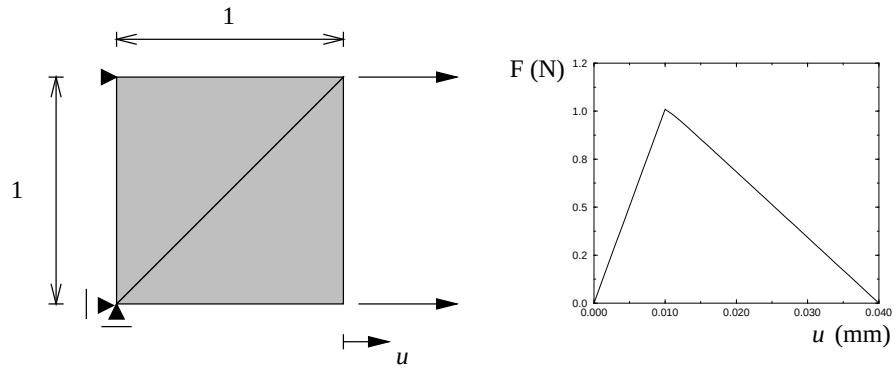

Figure 9: Patch arrangement and load–displacement response

triangles shown in Figure 9 is analysed with the following parameters: $f_t = 1.0\,\text{MPa}$, $E = 100\,\text{MPa}$, $\nu = 0.1$, $G_f = 0.02\,\text{Nmm/mm}^2$ (linear softening) and $\Delta u = 0.001$. In Figure 10 the damage parameter (ω) is plotted against the internal history variable (κ). The circles in Figure 10 show the result at the end of each displacement increment. As k becomes smaller, ω jumps from close to zero to very close to unity in one displacement increment. As a result, as k becomes smaller, it is not possible to calculate a reasonable derivative of ω with respect to κ without reducing the displacement increment to an unacceptably small value.

The increasing numerical difficulty in calculating a consistent tangent at the introduction of a discontinuity, as with the stress locking problem for the Rankine model, comes from the fictitious nature of the strain field. As k becomes smaller, the strains at the time of initiation of a discontinuity increase more rapidly, meaning that the consistent tangent for the discontinuity also varies very rapidly. Imposition of traction continuity then means that the very large strains are also complemented by a damage parameter that approaches unity. This has an adverse effect on the convergence behaviour and stability of the model. The construction of plasticity models in the stress space makes the robustness of such models less sensitive to the regularised displacement jump.

5 Conclusions

The application of continuum constitutive laws in strong discontinuity analysis hinges on the regularisation of the displacement jump, resulting in a bounded, although fictional, strain field. From the fictional strain field, spurious behaviour can arise unique to discontinuity analysis. The Rankine plasticity example illustrates that a negative hardening modulus does not guarantee satisfaction of the softening branch condition for all constitutive laws. The strain driven nature and the isotropy of the damage model applied here avoids the stress locking effects of the Rankine model, although the consequence is a deterioration of numerical stability and robustness as the displacement regularisation approaches a true discontinuity. Again, this is a result of the strain field within the discontinuity being a function of the regularisation function.

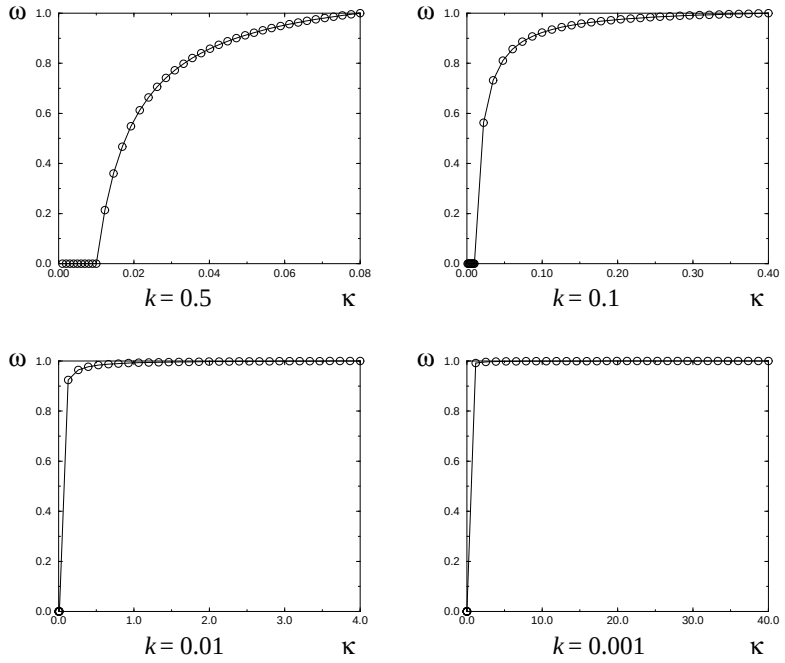

Figure 10: ω versus κ for varying k and constant Δu

By the nature of plasticity models, formulated in the stress space, they are prone to spurious stress development as a result of the displacement regularisation, although the stability of the numerical procedure is reasonably resilient to decreasing k. Conversely, damage models formulated in the strain space generally avoid k-dependent stress locking although stability can be compromised by decreasing k. For both plasticity and damage based models, the coupled behaviour of the discontinuity and the constitutive law must be examined for detrimental effects that do not arise in the classical continuum application of the constitutive laws.

Acknowledgments

This research is supported by the Technology Foundation STW, applied science division of NWO and the technology program of the Ministry of Economic Affairs, The Netherlands.

References

[1] E. Van der Giessen and R. de Borst. *Introduction to material instabilities in solids.* In: R. de Borst and E. van der Giessen (eds), Material Instabilities in Solids, 1–13, Delft, The Netherlands, (1998). Wiley.

[2] R. de Borst. *Nonlinear analysis of frictional materials.* PhD thesis, Delft University of Technology, (1986).

[3] E. C. Aifantis. *On the microstructural origin of certain inelastic models.* J. Eng. Mat. Tech., **106**, 326–334, (1984).

[4] R. de Borst, L. J. Sluys, H.-B. Mülhaus, and J. Pamin. *Fundamental issues in finite element analyses of localization and deformation.* Engng. Comp., **10**(5), 99–121, (1993).

[5] G. Pijaudier-Cabot and Z. Bažant. *Nonlocal Damage Theory.* ASCE J. Eng. Mech., **113**(10), 1512–1533, (1987).

[6] Z. Bažant and G. Pijaudier-Cabot. *Nonlocal Continuum Damage, Localization Instability and Convergence.* ASME J. Appl. Mech., **55**(2), 287–293, (1988).

[7] J. Oliver and J. C. Simo. *Modelling strong discontinuities by means of strain softening constitutive equations.* In: H. Mang, N. Bićanić, and R. de Borst (eds), EURO-C 1994 Computer Modelling of Concrete Structures, 363–372, Swansea, (1994). Pineridge Press.

[8] F. Armero and K. Garikipati. *Recent Advances in the Analysis and Numerical Simulation of Strain Localization in Inelastic Solids.* In: D. R. J. Owen, E. Oñate, and E. Hinton (eds), Computational Plasticity, Fundamentals and Applications, 547–561, Swansea, (1995). Pineridge Press.

[9] J. Mazars and G. Pijaudier-Cabot. *Continuum damage theory - application to concrete.* ASCE J. Eng. Mech., **115**(2), 345–365, (1987).

[10] R. Larsson and K. Runesson. *Element-embedded localization band based on regularized displacement discontinuity.* ASCE J. Eng. Mech., **122**(5), 402–411, (1996).

[11] P. H. Feenstra. *Computational aspects of biaxial stress in plain and reinforced concrete.* PhD thesis, Delft University of Technology, (1993).

[12] C. J. Pearce and N. Bićanić. *One multi-surface plasticity and Rankine model.* In: D. R. J. Owen and E. Oñate (eds), Computational Plasticity, Fundamentals and Applications, 957–964, Swansea, (1997). Pineridge Press.

[13] J. G. Rots. *Computational modeling of concrete fracture.* PhD thesis, Delft University of Technology, (1988).

[14] R. Tano, M. Klisinski, and T. Olofsson. *Stress locking in the inner softening band: A study of the origin and how to reduce the effects.* In: R. de Borst, N. Bićanić, H. Mang, and G. Meschke (eds), EURO-C 1998 Computer Modelling of Concrete Structures, 363–372, Rotterdam, (1998). Balkema.

[15] G. N. Wells. *Strong Discontinuity Analysis - The classical continuum.* Technical Report LR-TM-99-01, Delft University of Technology, Delft, The Netherlands, (1999).

[16] A. H. Berends, L. J. Sluys, and R. de Borst. *Discontinuous modelling of mode–I failure.* In: M. A. Hendrix, H. Jongedijk, J. G. Rots, and W. J. E. Spanje (eds), Finite Elements in Engineering and Science, 351–361, Rotterdam, (1997). Balkema.

[17] M. Jirásek. *Finite elements with embedded cracks.* Technical Report LSC Internal Report 98/01, École Polytechnique Fédérale de Lausanne, Switzerland, (1998).